Voltage dynamics of single-type voltage-gated ion-channel protein ensembles

Hanna Salman and Erez Braun*
Department of Physics, Technion-Israel Institute of Technology, Haifa 32000, Israel
(Received 2 December 1996)

Isolated ensembles of single-type voltage-gated potassium ion-channels are studied. The density of channels and the input current to the system are two control parameters in the experiments, while the voltage is the dynamical observable. The voltage fluctuations exhibit distinct behaviors in dense and dilute ensembles of channels. In dense ensembles, voltage fluctuations are constrained and exhibit relaxed oscillatory behavior, typical of a simple two-state system. At the other extreme of dilute ensembles, the complex many-state kinetics of the channel induces large-amplitude broad-spectrum voltage fluctuations. The effective number of channels that can respond to the voltage field is a dynamical variable, which determines the voltage stability and fluctuations and depends on the control parameters and the ensemble activity. The ensemble can move dynamically between two regimes of behavior with large and small effective numbers of channels. We study in detail these two regimes and the transition between them and show both by numerical simulations and by a simple analytic model how the coupling between the transmembrane voltage and the kinetics of channels leads to the observed dynamics. [S1063-651X(97)00607-7]

PACS number(s): 87.15.−v, 05.40.+j, 82.20.Mj

I. INTRODUCTION

Voltage-gated ion channels are transmembrane proteins that work as sophisticated selective stochastic switches for ionic currents in nerve and other excitable and nonexcitable cells [1]. The voltage-dependent switching of these channels between conducting and nonconducting states is a major factor in controlling the transmembrane voltage. In recent years, the fruitful combination of advanced molecular biology and electrophysiological techniques has enabled us to study in detail the kinetics of voltage-gated channels. In particular, the invention of the patch-clamp technique allows single channel recording, thus connecting directly measured macroscopic currents with single channel kinetics [2]. An important family of ion channels, the potassium-selective voltage-gated channels, are ubiquitous in cellular membranes. This family is of particular interest because of its important role in stabilizing the transmembrane voltage. Detailed studies have shown that many members of this family exhibit complex kinetics, indicating the existence of many states and transition rates, some of which are voltage dependent and some that are only weakly coupled to the transmembrane voltage or completely indifferent to it [1].

Generally, most of these potassium channels can be described by two separate branches of kinetics. One branch consists of closed (nonconducting) states coupled to one open (conducting) state via *fast*, voltage-dependent rates of transition. Here ''fast'' means on the millisecond time scale. On the other hand, the open state is also coupled, via voltage-independent (or weakly voltage-dependent) *slow* rates of transition, to inactive (nonconducting) states [1]. These inactive states (usually referred to as *C*-type inactivation [3]) can be distinguished from the closed states by their wide range of relaxation times that extend well beyond the millisecond regime. In this paper we use a simplified, schematic, three-state model [4] to represent a voltage-gated potassium channel: $C \leftrightarrow O \leftrightarrow I$, where C represents the closed states, O the open state, and I the inactive states.

Voltage-gated channels are usually studied by controlling the transmembrane voltage and monitoring the current (voltage-clamp technique) [2]. A different view of this system is achieved by studying the transmembrane voltage as a dynamical variable (current clamp), coupled to the kinetics through the voltage-dependent rates of the transition. The existence of inactive states, coupled to the open state via voltage-independent rates, may lead to nontrivial dynamics: The channel population in the $C \leftrightarrow O$ branch is depleted as more channels fall into the inactive states, from which their relaxation is stochastic and very slow. The depletion process becomes increasingly dominant with higher channel activity: The longer a channel spends in the open state, the more likely it is to inactivate. Since the channel distribution among the states determines the transmembrane voltage, it is clear that the variety of time scales arising from the multiplicity of states (in particular, the inner structure of the I states) leads to modulations of the transmembrane voltage as a function of the channels' history of activity.

In an isolated biological system, composed of one species of ion channels, one can ask the following question: How do the many microscopic functional degrees of freedom of the underlying proteins interact with the macroscopic field that couples them? Put differently, the ion channels, in a simplified system, are identical stochastic elements whose collective interaction with the macroscopic voltage field depends on the microscopic functional configurations available to them. How these microscopic degrees of freedom show up in the macroscopic dynamics is the focus of this paper. In this paper we summarize a set of experiments designed to study the voltage dynamics in ensembles of *single*-type voltage-gated ion channels. Combining molecular biology and patch-clamp techniques, controlled ensembles of single-type voltage-gated potassium channels are constructed and studied in isolated patches of membrane, *detached from any in-*

*Author to whom correspondence should be addressed.

tracellular or biochemical effects. The number of channels in the ensemble and the external current stimuli to the membrane are used as control parameters.

The present study follows two recent publications, where we have shown that in an isolated ensemble of single-type potassium channels one can link directly the kinetics of the underlying channels to the transmembrane voltage and its fluctuations [4,5]. The main observations can be summarized as follows.

(i) Above a certain number of channels (determined by the various parameters of the system), the transmembrane voltage is stabilized around a typical value, set by the voltage-dependent kinetics of the closed-open transitions. The voltage fluctuations are constrained by a feedback mechanism between the voltage and the kinetics and exhibit relaxed oscillations that are identified in the power spectrum and the voltage autocorrelation function. A direct interpretation of these results leads to a simple model that presents the voltage fluctuations in an ensemble of voltage-gated channels as a damped harmonic oscillator driven by white noise [5]. The voltage response of a dense ensemble of channels to small-amplitude sinusoidal current stimuli exhibits relaxed oscillations with characteristic time scales comparable to those measured from the noise autocorrelation at a zero holding current.

(ii) When the number of channels in the ensemble is small (defined more accurately below), the complex kinetics of the channel, including the stochastic transitions into and out of the inactive states, plays a significant role and the transmembrane voltage exhibits large-amplitude, broad-spectrum fluctuations.

(iii) The stability of the transmembrane voltage, even for dense ensembles of channels, is, however, only marginal. A large enough external input current, forcing an increase in the number of open channels, may lead to a continuous drift in voltage. This instability is due to loss of channels into the inactive states, from which the relaxation is much slower than the characteristic time scale of voltage dynamics. Subject to a sufficient high holding current, the inactive states work as a sink for channels, causing an ensemble with large numbers of channels to behave as if it has only a small number of channels. Thus, as we elaborate below, the number of channels in the $C \leftrightarrow O$ branch of the kinetics compared with the number of open channels determines the dynamics rather than directly the total number of channels in the ensemble.

This manuscript is organized as follows. In Sec. II we summarize the experimental methods. In Sec. III we discuss the transmembrane voltage and its fluctuations. In Sec. IV we study ensembles with a large number of channels and their response to external stimuli. In Sec. V the other extreme of ensembles with a small number of channels is presented. We summarize and discuss these results in Sec. VI.

II. EXPERIMENTAL METHODS

The experimental setup [see Fig. 1(a)] consists of a small patch of membrane ($\sim 2\ \mu m^2$) containing a certain density of single-type voltage-gated potassium channels. A sample preparation is described in detail elsewhere [4]; we give here only a brief summary of it.

The potassium-selective voltage-gated channel *Shaker IR*

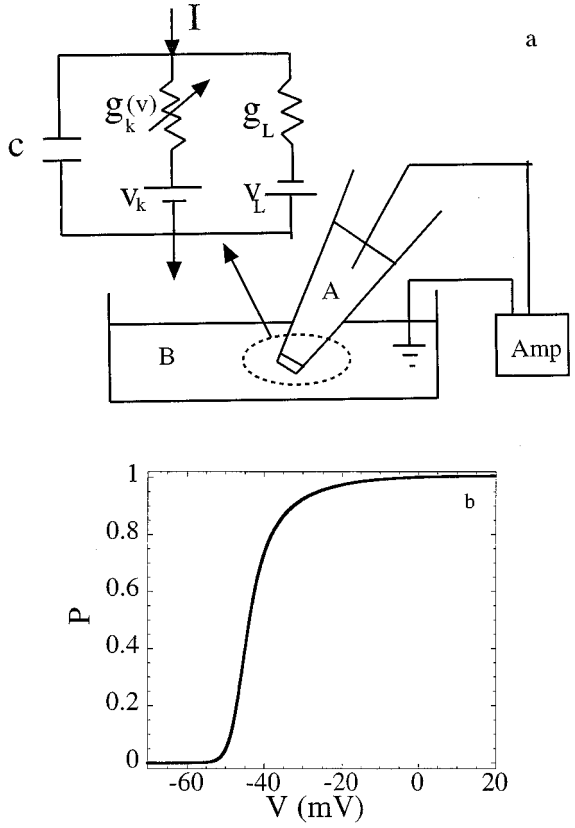

FIG. 1. (a) Schematic description of the experimental setup and an equivalent electrical circuit containing membrane capacitance c, leak conductivity g_L, channel conductivity $g_k(V)$, and two voltage sources V_L and V_k determined by the leak and potassium reversal potentials and set by the ionic concentration gradients across the membrane. The concentration gradients are between the pipette solution A and the bath solution B (see the experimental methods in text). I is the holding current set by the patch-clamp amplifier in the current clamp mode. (b) Steady-state fraction of open channels $\alpha/(\alpha+\beta)$ computed with the rates given in [14] as a function of the transmembrane voltage.

[3,4,6] is expressed in the membrane of a *Xenopus* oocyte (a developing frog's egg). This channel is a mutant of the original delayed-rectifier *Shaker* channel and does not exhibit the fast inactivation existing in the latter. In addition, a point mutation F425G was introduced in it [7]. This particular channel was chosen because it can be expressed in a very wide range of densities without any apparent effects on the kinetics. The channel exhibits typical fast-activating and slowly inactivating behavior. To prepare an ensemble of ion channels, cRNA coding for the channel, at various concentrations, is injected into a *Xenopus* oocyte. Methods of DNA and cRNA preparation are standard molecular biology techniques [8]. Oocytes are harvested from mature *Xenopus* females and dissociated in 2 mg/ml of collagenase 1A (Sigma). Stage V-VI defolliculated cells are then injected with 0.4–40 nl of mRNA (~ 1 mg/ml). Injected cells are incubated at 18 °C for up to 7 d in frog Ringer's solution. The variability in expression of channels among different membranal regions of a single oocyte (at which only a small patch of membrane is used in a single experiment; see below) and between different oocytes enables us to scan more than three decades of channel densities.

All the experiments presented here were carried out on detached patches, using standard patch-clamp techniques. By using glass pipettes (AM Systems Inc., WA, No. 7052), pulled and polished to a micrometer size (with a typical resistance in the range of $3-5\,\mathrm{M}\Omega$), a small patch of membrane can be detached from the oocyte after the establishment of a tight seal (resulting in 10–100 GΩ leak resistance). In that way, the experiments reflect processes that are inherent to the ensemble of channels, dissociated from intracellular effects. The capacitance of the system is largely determined by the glass pipette, and it was reduced to ~ 1 pF by exposing the glass to the bath solution only at its tip. The pipette solution contained (in mM) 96 NaCl, 2 KCl, 1 $CaCl_2$, 1 $MgCl_2$, and 10 Hepes. The bath solution contained 95 KCl, 5 NaCl, 1 EGTA, and 10 Hepes. Both solutions were at *p*H 7.5. All the experiments were performed in the inside-out configuration at room temperature. An Axopatch 200 A amplifier (Axon Instruments, Foster City, CA) was used with its output filter set at 5–10 kHz. The bias current of the amplifier under a current clamp is 0.3 pA and is stable during and in between experiments. The data were recorded using a pulse-code modulator (Neuro Data Instruments, model DR-390, 14 bit).

A detailed study of the kinetics of this channel was carried out under a voltage-clamp and was published elsewhere [4]. The number of voltage-gated channels in the patch of membrane, in each experiment, was measured in the voltage-clamp mode by monitoring the maximal conductivity of the membrane (the slope of the I-V curve between $+50$ and $+70$ mV) and dividing it by the single channel conductivity g_k of 0.013 pA/mV [9]. The leak conduction g_L was measured in the voltage-clamp mode at the beginning and end of each experiment to verify the stability of it. In all the experiments presented here it had values in the range 0.01–0.07 pA/mV.

III. THE TRANSMEMBRANE VOLTAGE AND ITS FLUCTUATIONS

Voltage-gated potassium channels stabilize the membrane resting potential in many excitable and nonexcitable cells (see [4] and references therein). Let us first describe the behavior of the transmembrane voltage and its fluctuations for a patch of membrane with different numbers of voltage-gated potassium channels at zero holding current. In addition to the voltage-gated channels, the membrane possesses a constant leak conductance that is voltage independent. Figure 1(a) presents an equivalent electrical circuit for the experimental system. Without external stimuli, the resting potential is determined, dynamically, by the requirement for total zero current, which is translated into a balance between the leakage current and the channels current:

$$g_L[V-V_L]=g_k(V)[V-V_k],$$

where $g_L, g_k(V)$ are the leak and voltage-dependent conductances, respectively, and V_L, V_k are the leak and potassium reversal potentials, respectively. We have shown recently that the resting potential drops sharply to more negative (hyperpolarized) values as the number density of voltage-gated potassium channels in the ensemble is increased [4]. Above a certain characteristic number of channels, the steady-state transmembrane voltage almost saturates around -60 mV. This characteristic number of channels depends on the various parameters of the system, especially the leak conductance. In our system, it has a value of approximately 50 channels (conductivity of 0.46 pA/mV) [4]. The sharp drop in potential for small numbers of channels and its saturation for large numbers of channels is a direct consequence of the voltage-dependent kinetics of the channels. It follows the steady-state fraction of open channels as a function of transmembrane voltage, which has a sharp increase above ~ -50 mV and an exponential tail at lower values of voltage [see Fig. 1(b) for the description of this function]. For the model system used in our experiments, with single-type potassium channels, it is easy to show the direct connection between the single channel's kinetics and the transmembrane potential.

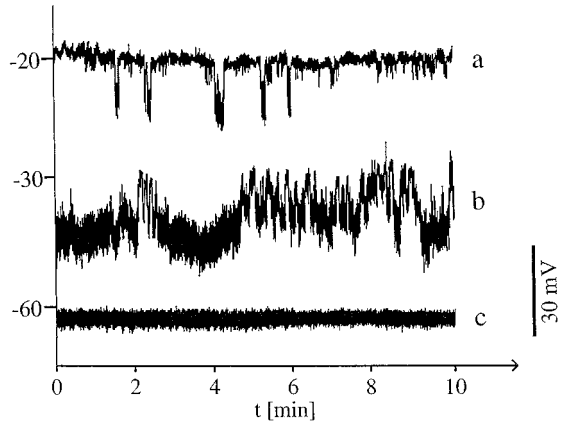

FIG. 2. Voltage traces, 10 min long, at zero holding currents for patches of membrane with different numbers of voltage-gated ion channels. The membranes contain (a) 19, (b) 40, and (c) 4000 channels for traces *a*, *b*, and *c*, respectively.

Figure 2 shows three voltage traces, at zero external holding currents, for three patches of membrane with different numbers of channels. In trace *a* the number of channels is approximately 19 and is so low that the resting potential is stabilized around the leak reversal potential and escapes from it stochastically to more negative values (by more than 20 mV) due to opening of channels. In trace *b* there are approximately 40 channels, some of which are always active, but the potential exhibits large, irregular fluctuations, with slow modulations. Trace *c* has been recorded from a patch of membrane containing approximately 4000 potassium channels so the transmembrane voltage is stable and exhibits low-amplitude fluctuations. Note that the average number of open channels is, in all three cases, small compared to the total number of channels in the ensemble. In trace *a* there are 2–3 open channels, in trace *b* 3–4 open channels, and in trace *c* around 10 open channels. Thus, what determines the dynamics is not the total number of channels, which is always large compared to the number of open ones, but rather the number of *available* channels, i.e., those in the $C \leftrightarrow O$ branch of the kinetics, compared to the required number of open channels. We shall see that for a large number of available channels the transmembrane voltage fluctuations reflect the fast, voltage-dependent $C \leftrightarrow O$ transitions. In contrast, for a small number of available channels the slow, voltage-

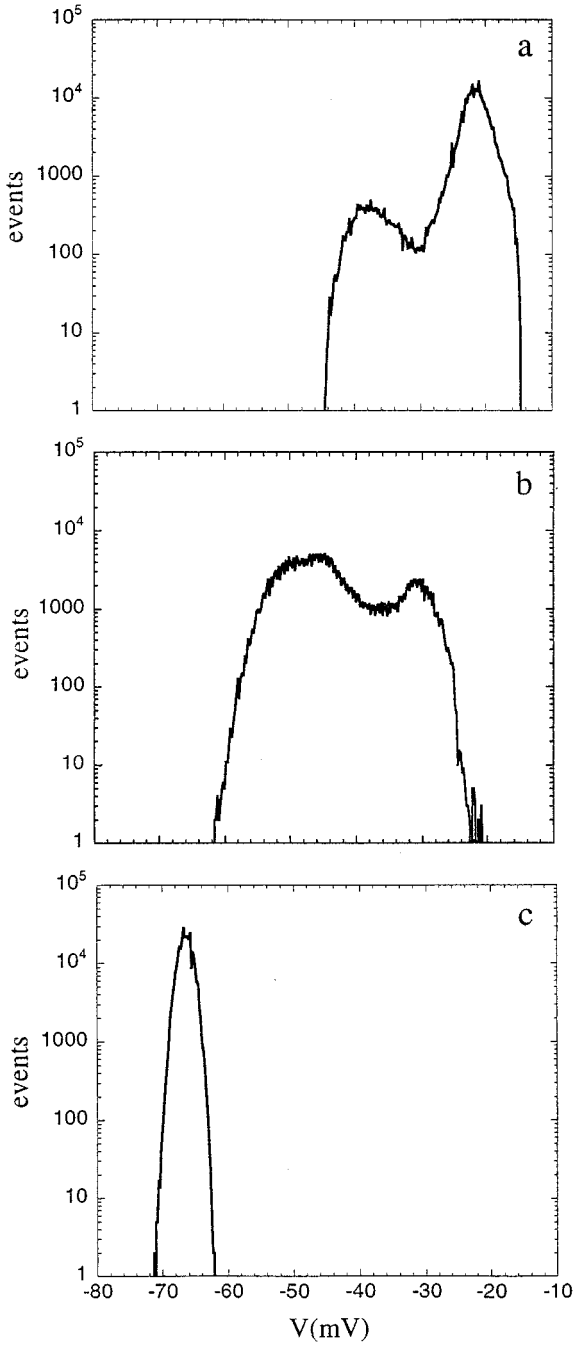

FIG. 3. Histograms of voltage fluctuations for the three voltage traces of Fig. 1.

independent $O \leftrightarrow I$ kinetics intervenes with the fast transitions and lead to large fluctuations with complex spectral characteristics. Figure 3 shows voltage histograms computed for the traces of Fig. 2. The first two are typically wide and multi-peaked, while the last one fits a narrow Gaussian distribution. We now discuss in detail the two extremes of large and small numbers of voltage-gated channels.

IV. LARGE NUMBERS OF AVAILABLE CHANNELS

A. Two-state model

The dynamics is considerably simplified by working with ensembles containing large numbers of voltage-gated channels. Under these conditions, the complexity of the inactive states does not influence the dynamics significantly. We have shown recently that such a system can be described by a two-state $C \leftrightarrow O$ model and exhibits characteristic spectral properties that reflect the feedback between the transmembrane voltage and the voltage-dependent rates of the transition [5]. To summarize briefly, the channels are modeled as particles occupying an asymmetric double-potential well, which represents the closed and open states. The barrier is voltage dependent and represents the opening and closing transition rates. The main result is twofold. First, a fluctuation in the distribution of channels between the wells is coupled to the height of the barrier and causes the voltage noise to exhibit relaxed oscillations. Second, the amplitude of the voltage noise is reduced, in *absolute* terms, when the number of channels in the ensemble is increased or when a positive dc current is applied to the membrane forcing a small increase in the average number of open channels.

We begin with two coupled first-order differential equations for the transmembrane voltage and the fraction of open channels. Linearizing these equations around their steady-state values yields a picture of the ensemble's voltage fluctuations as a damped harmonic oscillator, driven by a noise term.

A two-state kinetic model for the voltage-gated ion channel

$$C \underset{\beta(V)}{\overset{\alpha(V)}{\rightleftarrows}} O \tag{1}$$

leads to the equations

$$c dV/dt = -[g_k^* N p (V - V_k) + g_L (V - V_L)] + I, \tag{2}$$

$$dp/dt = \alpha(V) - \lambda(V) p + \xi. \tag{3}$$

Here V is the transmembrane voltage, c is the membrane capacitance, g_k^* is the single channel conductivity, N is the total number of channels in the ensemble, p is the fraction of open channels (the same as the probability of a single channel to be in the open state), I is the external holding current, $\lambda(V) = \alpha(V) + \beta(V)$ is the relaxation rate of the two states (shown in the inset to Fig. 4), and ξ is a noise term, of thermal origin, which in principle may depend on the mean transmembrane voltage and the kinetics and is assumed here to be Gaussian and white. Thus we note that the equation for the fraction of open channels (which is proportional to the potassium conductivity of the membrane) is modeled here as a Langevin equation. The introduction of the noise term (with the dimensions of rate) in this form is *ad hoc*. No noise term is added to the voltage equation since we have shown [5] that the voltage noise in a patch of membrane containing no voltage-gated channels is at least two orders of magnitude smaller than the voltage noise generated by conduction fluctuations of voltage-gated channels. Thus contributions from Johnson and other sources of noise are negligible compared to that of the channels. The channels are assumed to fluctuate independently between the two states, so that the only correlations are introduced through the coupling of the kinetics to the voltage.

The noise term is related to the damping term in the dynamic equation for the fraction of open channels and can be computed under certain assumptions. In particular, for small fluctuations $p=\overline{p}+\rho$, where $\overline{p}$ is the mean fraction of open channels and $|\rho| \ll \overline{p}$, Eq. (3) yields

$$d\rho/dt = -\lambda(V)\rho + \xi. \tag{4}$$

The noise term is assumed to be δ correlated $\langle \xi(t)\xi(t+\tau)\rangle = A\delta(\tau)$ with zero mean and A can be computed by comparing the solution of the macroscopic equation with a direct calculation of independently fluctuating channels at steady state. A similar calculation was presented in [10]. The solution of the dynamic equation (4) gives

$$\rho(t) = \int_0^t e^{-\lambda(t-\tau)}\xi(\tau)d\tau + \rho(0)e^{-\lambda t}, \tag{5}$$

where the last term is the decay of initial conditions and can be neglected for asymptotically long times. The variance of fluctuations is then

$$\overline{\rho(t)^2} = \frac{A}{2\lambda}(1-e^{-2\lambda t}). \tag{6}$$

On the other hand, a direct calculation of N independently fluctuating channels gives

$$\overline{\rho(t)^2} = \frac{1}{N}\overline{p}(1-\overline{p}). \tag{7}$$

Finally, a comparison of the long-time behavior gives

$$A = \frac{2\lambda(\overline{V})}{N}\overline{p}(1-\overline{p}). \tag{8}$$

Thus the voltage dependence of the noise is expressed in terms of the relaxation rate of the two states and the average fraction of open channels. Though very weak, this dependence may nevertheless introduce nonlinearity in the model.

Assuming small fluctuations around steady state $p=p_s+\rho$ and $V=V_s+v$, where

$$\overline{p} = p_s = \frac{\alpha_s}{\lambda_s}, \qquad V_s = \frac{g_k^* N p_s V_k + I}{g_k^* N p_s + g_L}, \tag{9}$$

we can linearize the model [Eqs. (2) and (3)]. The dynamics of fluctuations is determined by

$$\frac{dv}{dt} = f_{11}v + f_{12}\rho, \tag{10}$$

$$\frac{d\rho}{dt} = f_{21}v + f_{22}\rho + \xi. \tag{11}$$

Here

$$f_{11} = -\tau_0^{-1}[\tilde{g}_k N p_s + 1], \qquad f_{12} = -\tilde{g}_k N \tau_0^{-1}[V_s - V_k], \qquad f_{21} = -\lambda_{,v}p_s + \alpha_{,v}, \qquad f_{22} = -\lambda_s, \tag{12}$$

where $\alpha_{,v}$ and $\lambda_{,v}$ are the time derivatives of the transition rates at the steady-state voltage, $\tau_0 = C/g_L$ is the characteristic capacitance time of the membrane, and $\tilde{g}_k = g_k^*/g_L$ is the normalized conductivity of a single potassium channel. Without loss of generality, we take $V_L = 0$. Finally, we combine the dynamic equations (10) and (11) into one equation for voltage fluctuations [5]

$$\frac{d^2v}{dt^2} = -\gamma\frac{dv}{dt} - \omega_0^2 v + R. \tag{13}$$

The voltage fluctuations perform damped harmonic oscillations, with a damping coefficient and a natural frequency given by

$$\gamma = \tau_0^{-1}[\tilde{g}_k N p_s + 1] + \lambda_s, \qquad \omega_0^2 = \tau_0^{-1}(\{\tilde{g}_k N[V_s - V_k]\}\{\alpha_{,v} - \lambda_{,v}p_s\} + \lambda_s[\tilde{g}_k N p_s + 1]), \tag{14}$$

driven by a noise term

$$R = -\tilde{g}_k N \tau_0^{-1}[V_s - V_k]\xi. \tag{15}$$

An intuitive feeling for this behavior is provided by the following argument. A fluctuation in the distribution of channels between the closed and open states, decreasing the number of open ones, causes an extra current that charges the membrane and leads to an increase in the transmembrane voltage. This in turn affects the distribution of channels with a crucial phase lag, which results in oscillatory behavior, damped by the relaxing nature of the potassium channels (i.e., driving the voltage back to lower values). Similar behavior can be found in other physical systems. In some lasers, for example, the phase lag between the buildup of the photon population inside the cavity and the pumping rate leads to relaxed oscillations when the laser is switched on [11]. In our case, the conduction fluctuations of the channels continuously drive these relaxed oscillations. As shown in a previous publication [5], the capacitance time τ_0 and the charging power of a single channel $\tilde{g}_k$ determine the voltage response time. The interplay between the barrier fluctuations (determined by voltage dynamics) and the residence time of channels in the potential wells is reminiscent of other activation phenomena in modulated potentials [12].

The solution to the problem of a Brownian particle bound to the origin by a harmonic force is standard and appears in many textbooks (see, for example, [13]). We summarize here the main features of this model and then discuss these results in the context of voltage-gated potassium channels. The autocorrelation function for voltage fluctuations is given by

$$\langle v(t)v(0)\rangle = \frac{\pi R_{\overline{\omega}}}{\gamma\omega_0^2}\left(\cos\omega_1 t + \frac{\gamma}{2\omega_1}\sin\omega_1 t\right)e^{-\gamma t/2}, \tag{16}$$

where

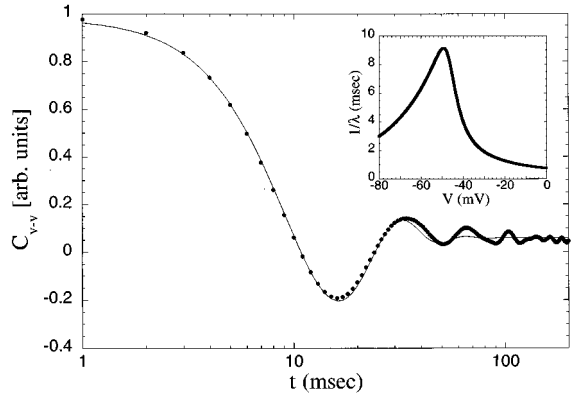

FIG. 4. Normalized voltage autocorrelation function averaged over 80 sec for a patch of membrane containing 3600 channels at a zero holding current. The solid line is the best fit to the data obtained from the autocorrelation of a damped harmonic oscillator [Eq. (16)] with $2\pi\omega_1^{-1}=32.6$ msec and $\gamma^{-1}=6.5$ msec. The inset shows the relaxation time $1/\lambda=1/[\alpha(V)+\beta(V)]$ versus the transmembrane voltage, calculated with the values in [14]. Note the peak of this function at around 9 msec and -50 mV, which is at the relevant window for the ensembles of channels in the experiments.

$$\omega_1=\left(\omega_0^2-\frac{\gamma^2}{4}\right)^{1/2} \tag{17}$$

is the characteristic oscillatory frequency and $R_{\overline{\omega}}=-f_{12}A/2\pi$ is the power spectrum of the noise. The power spectrum of the voltage fluctuations is then given by

$$|(v_\omega)|^2=\frac{R_{\overline{\omega}}}{(\omega_0^2-\omega^2)^2+\gamma^2\omega^2}, \tag{18}$$

with the variance

$$\langle v^2\rangle=\frac{\pi R_{\overline{\omega}}}{\gamma\omega_0^2}. \tag{19}$$

We now use these results to analyze the experimental measurements of voltage fluctuations.

B. Experimental results

A typical voltage autocorrelation function measured for a patch of membrane containing 3600 voltage-gated channels at a zero holding current is shown in Fig. 4. The autocorrelation function is computed by direct summation of a digitized voltage trace

$$\langle V_iV_{i+\varphi}\rangle=\frac{\Sigma_i(V_i-\overline{V})(V_{i+\varphi}-\overline{V})}{\Sigma_i(V_i-\overline{V})^2}. \tag{20}$$

Here V_i is the digitized voltage at point i with a millisecond resolution and V is the mean voltage. The autocorrelation is averaged over 80 sec. The solid line is the best fit to the autocorrelation of a damped harmonic oscillator, predicted by the linearized model above [Eq. (16)]. The voltage fluctuations exhibit relaxed oscillations with characteristic time scales of $2\pi\omega_1^{-1}=32.6$ msec and $\gamma^{-1}=6.5$ msec, which can be compared with the characteristic time scale of the channel's kinetics (inset of Fig. 4) of about 9 msec. Figure 5 summarizes the dependence of the damping time scale γ and the oscillatory time scale $\omega_1/2\pi$ on the total number of voltage-gated channels in the membrane. The large variability in the results reflects the differences in capacitance times of the different patches of membrane. In general, all the characteristic time scales become smaller with the increase in the number of channels in the ensemble. Figures 6(a) and 6(b) show the dependence of the characteristic time scales on the number of channels and the capacitance time, respectively, for the linearized model [Eqs. (14) and (17)]. The characteristic time scales decrease with the number of channels. This sensitivity is greatest in the lower range of numbers of channels, which is the relevant range for the experiments. The transition between underdamped $\omega_0^2>\gamma^2/4$ and overdamped $\omega_0^2<\gamma^2/4$ behavior is possible only for very large (or very small, see [5]) capacitance times [ω_1 goes to zero in Fig. 6(b)]. Such a transition marks a time-scale separation between the voltage dynamics (barrier fluctuations) and the kinetics (channel resident time) and is typical of similar activation phenomena [5,12]. The oscillatory frequency ω_1 and

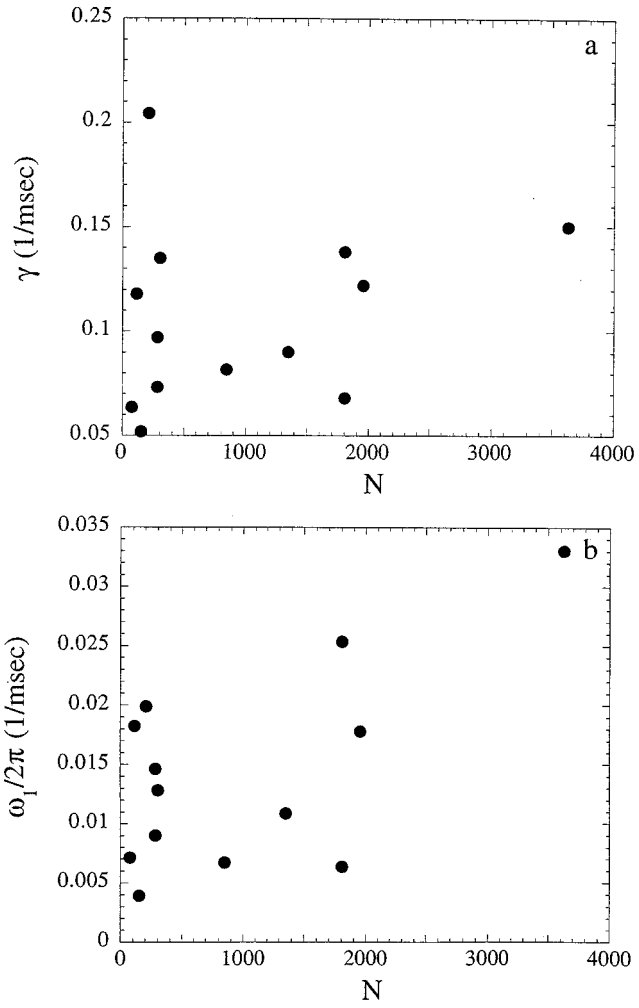

FIG. 5. Characteristic time scales (a) γ and (b) $\omega_1/2\pi$ for different patches of membrane containing different numbers of channels at zero holding currents. The time scales are computed by fitting the measured voltage autocorrelation to the one derived from the model of damped harmonic oscillator [Eq. (16)].

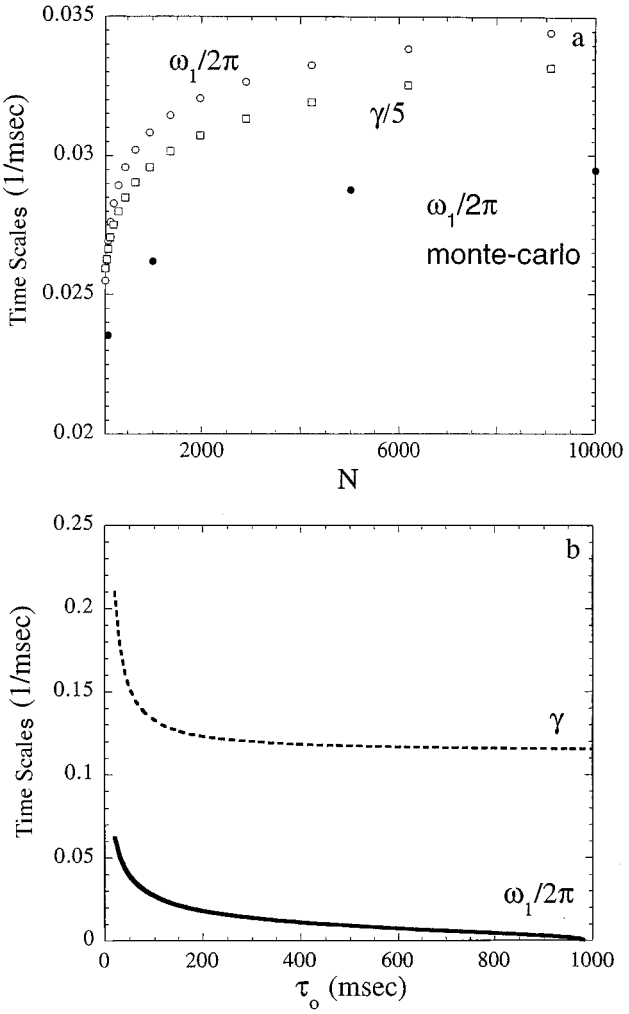

FIG. 6. (a) Characteristic time scales γ (squares) and $\omega_1/2\pi$ (circles) calculated from the linear model, as explained in the text, as a function of the number of channels in the membrane. γ is divided by 5 to bring it to the same scale as $\omega_1/2\pi$. Shown with dots are the $\omega_1/2\pi$ obtained by fitting the autocorrelation function of the damped harmonic oscillator to the one computed from the voltage fluctuations of a Monte Carlo simulation of 100 channels with two states ($C \leftrightarrow O$). The parameters of the simulations are $\tau_0 = 100$ msec, $g_k = 0.5$ in units of the leak conductivity, and the rates as in [14]. (b) Characteristic time scales γ (dashed line) and ω_1 (solid line) calculated from the linear model, as a function of the capacitance time $\tau_0 = C/g_L$. Note that ω_1 goes to zero above $\tau_0 \approx 900$ msec, marking the transition between underdamped and overdamped systems.

the friction coefficient γ can be computed by solving Eq. (2) numerically with the kinetics described in Eq. (1). By using a Monte Carlo simulation the noise is automatically taken care of and nonlinear effects are included. The probability of each channel to make a transition out of its state, at the time interval t, $t+dt$, is computed by $P = 1 - e^{-kdt}$, where k is the relevant rate of the transition [14]. This probability is compared to a random number, pulled out of a uniform distribution [15], and a transition is made if the random number is smaller. A voltage trace is simulated by solving a difference equation derived from Eq. (2) between t and $t+dt$, using the fraction of open channels derived from the procedure above at each time step. We then compute the voltage autocorrelation function for a simulated voltage trace, fitting it with the autocorrelation of a damped harmonic oscillator [Eq. (16)], and extract the characteristic time scales predicted by the nonlinear model. The oscillatory frequencies ω_1 thus computed are shown by dots in Fig. 6(a). Although the numbers are not exactly the same as in the linearized model above, the general dependence on the number of channels is approximately reproduced by the nonlinear Monte Carlo simulations. The small deviation of the characteristic time scale predicted by the linear model and the one computed in the simulations indicates the existence of (weak) nonlinear effects in the system. The same conclusion was reached in [5] by comparing the variance of voltage fluctuations computed from Monte Carlo simulations with the one predicted by the linear model.

The two-state model presented above assumes the dynamics as determined by a deterministic part plus a stochastic term. This division lies at the basis of the Langevin approach. There is, however, no fundamental basis for it in the case of ion channels. In order to obtain more insight into the relation between the deterministic and stochastic sources of the dynamics, the response of the ensemble of channels to external periodic stimuli was studied and its time scales compared to the ones computed from the spontaneous noise autocorrelation. Figure 7(a) shows part of a long voltage trace (solid line), measured under a current-clamp condition, for a patch of membrane containing ~ 300 voltage-gated potassium channels and driven by an external sinusoidal current of 2 pA rms amplitude at 3 Hz (dotted line). Compared to the leakage current at steady state (~ 3.4 pA), this stimulus may be considered as a small perturbation. Only the upper trace is shown; the lower part follows a sinusoidal curve in phase lag with the current stimulus. Note that due to the steep dependence of the kinetics of channels on voltage [this function is shown in Fig. 1(b)] there is only a relatively narrow window of time in which channels respond to the stimulus. Thus, although the stimulus frequency (3 Hz) is low compared to the transition rates of channels (in the kilohertz regime), it is still marginal. Higher frequencies, as we shall see, compete with the kinetics. The voltage peaks observed in response to the stimulus appear to have irregular phases. For stimulus frequencies, which do not intervene with the kinetics of the channels, at least three separate voltage peaks can be discerned. Figure 7(b) shows the phase histogram ($t = 0$ when the current stimulus crosses zero with a positive slope) for the same trace as in Fig. 7(a), computed over 80 sec. The first peak is always relatively narrow and synchronized with the stimulus, while the second and third peaks are wider. This is a clear signature of the stochastic response of the channels. As we shall see below, although the voltage response to the external low-amplitude driving current is very noisy, the average time lapse between the peaks represents a well-defined deterministic response of the system.

Increasing the stimulus frequency beyond 3–4 Hz leads to strong intervention with the kinetics of channels. Figure 8(a) shows the average time lapse between the first and second peaks as a function of the stimulus frequency for different patches of membrane containing different numbers of voltage-gated channels. The mean time lapse between the peaks drops sharply with the frequency for frequencies above 3–4 Hz. Figure 8(b) shows the ratio between the number of

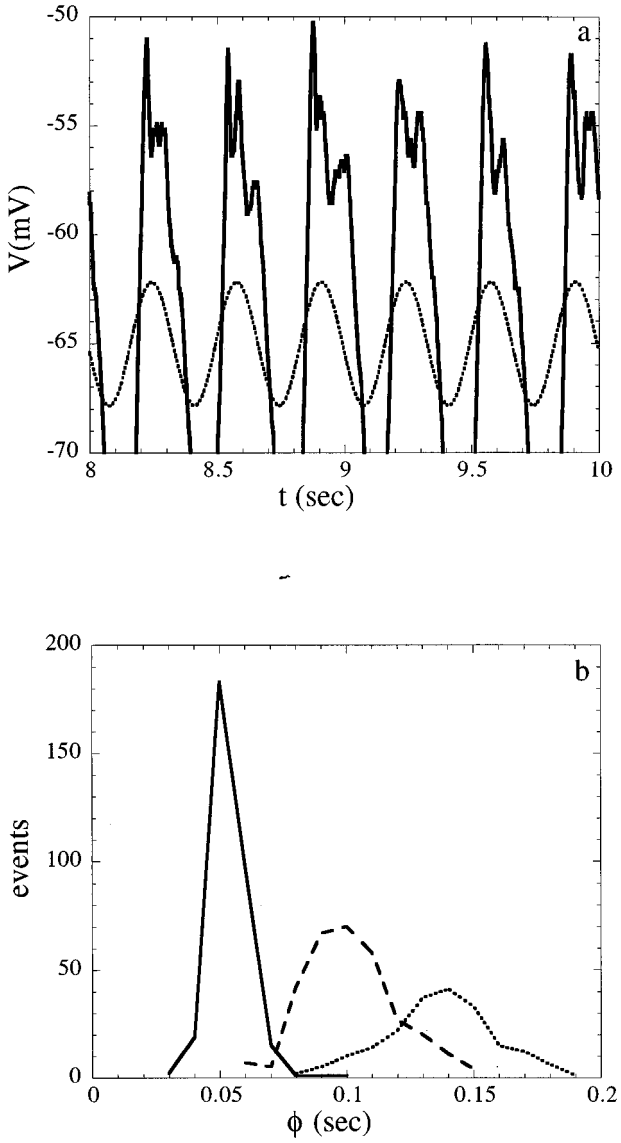

FIG. 7. (a) Small section of a voltage trace recorded from a patch of membrane containing 300 channels and stimulated by a sinusoidal current of 2 pA rms and a frequency of 3 Hz (dotted line). Note the peaks that appear in the voltage trace. Only the upper half of the voltage response is shown; the lower half follows the current input with a constant phase lag. (b) Phase histograms of the first (solid line), second (dashed line), and third (dotted line) peaks computed from an 80-sec voltage trace, part of which is shown in (a). Note that the second and third peaks are wider than the first one. The phase Φ is measured relative to the zero crossing point of the input current with a positive slope.

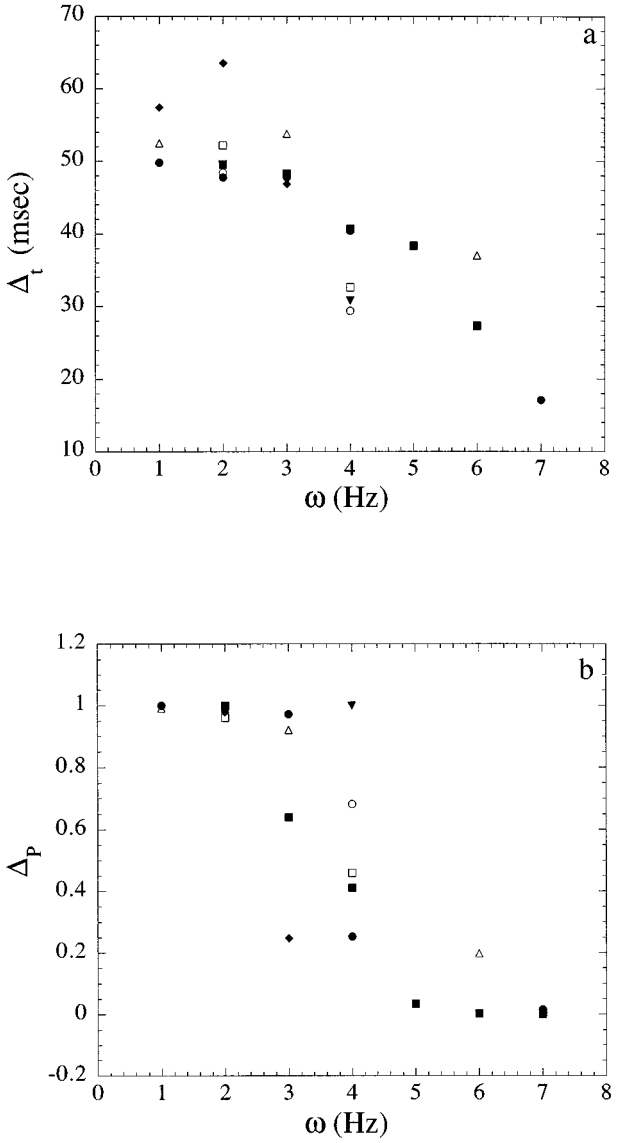

FIG. 8. (a) Mean time lapse Δ_t, between the first and second peaks and (b) ratio between the number of second peaks to the number of first peaks Δ_p from voltage traces of patches of membrane containing large numbers of channels and stimulated by sinusoidal currents of 2 pA rms, as a function of the stimulation frequency. The different patches of membrane contain 112 (filled triangles), 206 (circles), 282 (diamonds), 300 (empty triangles), 1352 (filled squares), 1803 (dots), and 2216 (empty squares) channels. Note the large changes in the frequency range 3–4 Hz.

second peaks to the number of first peaks, for different frequencies. It leads to the same conclusion: Above 3–4 Hz there is a sharp drop in the occurrence of a second peak in the trace, implying that at higher frequencies the stimulus competes with the kinetics and strongly affects the response. This behavior is not due to the voltage at the peaks, as can be seen in Figs. 9(a) and 9(b), which show the average voltage of the first peak and the average ratio between the voltages of the first and second peaks, respectively, as functions of the stimulus frequency. Thus the reason for the decrease in the separation of peaks and the number of times it appears is due to the fact that at higher frequencies there is less time in the relevant voltage window for the channels to respond. At high enough frequencies, the peaks that do show up synchronize with the stimulus. At low frequencies, the average time lapse between the first and second peaks in the experiments was found not to depend sensitively on the amplitude of the stimulus. We conclude that at frequencies up to 3 Hz and at the low-amplitude driving currents used in these experiments, the average time lapse between the first and second peaks in the voltage response (Δ_t) can be taken as a reliable measure of the characteristic time-scale response of the ensemble of channels to external stimuli, independent of the stimulus itself. For a linear response, we expect to find $\Delta_t = 2\pi/\omega_1$.

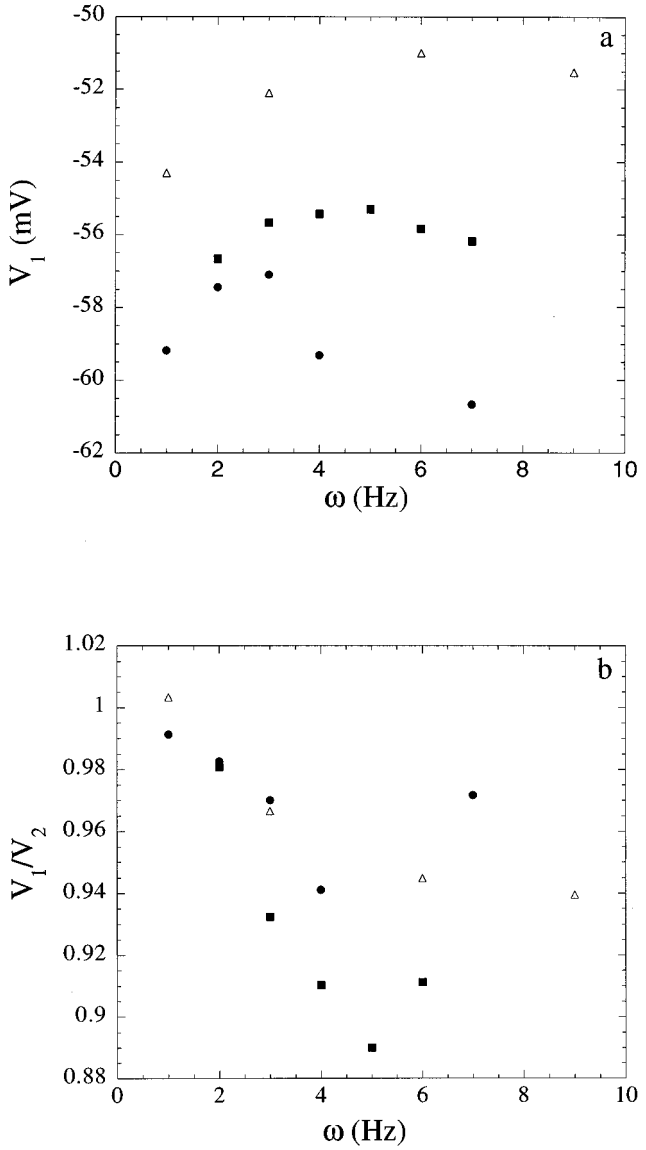

FIG. 9. (a) Voltage of the first peak and (b) ratio between the voltage of the first to the second peak for the same patches of membrane as in Fig. 8, as a function of the stimulation frequency.

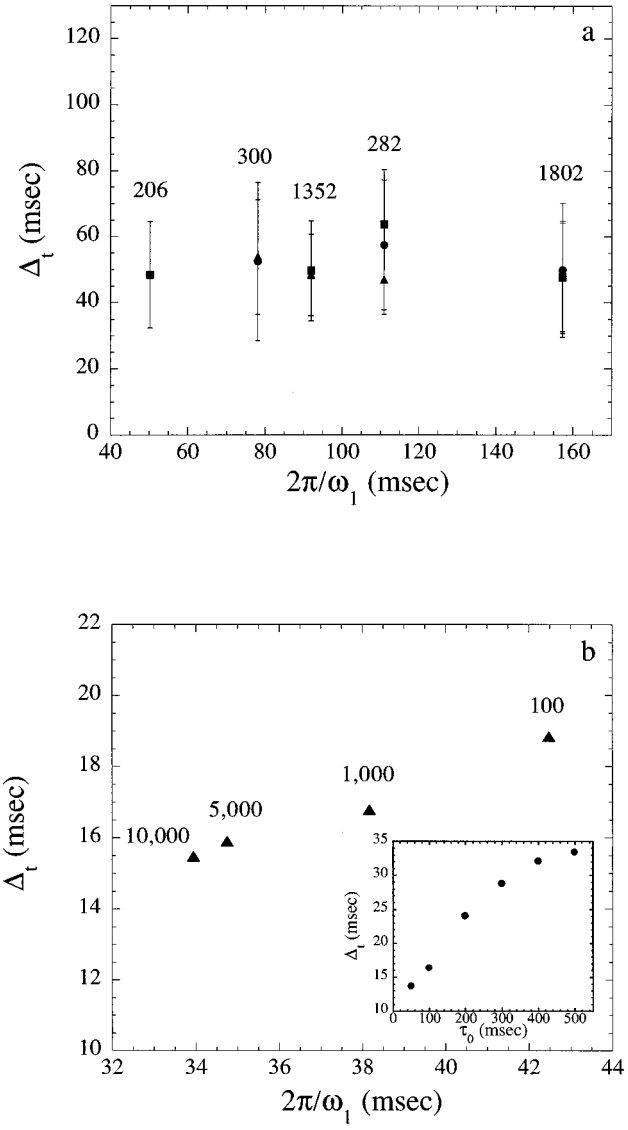

FIG. 10. (a) Comparison between the time scale for the response of the ensemble of channels to sinusoidal current stimulation Δ_t and the characteristic oscillatory time scale $2\pi/\omega_1$ derived from fitting the measured voltage autocorrelation function, at zero current, with the ones of the damped harmonic oscillator [Eq. (16)]. Each patch of membrane (with number of channels as marked) is measured at zero current for at least 1 min and then stimulated by a sinusoidal input current at different frequencies (up to 3 Hz) and 2 pA rms amplitude. The error bars represent the standard deviation in Δ_t. (b) Same as in (a), but for Monte Carlo simulations of 100, 1000, and 10 000 channels having the two-state kinetics [14]. The inset shows the average time separation Δ_t between the first and second peaks from a numerical solution of the model [Eqs. (2) and (3)] with no noise term, as functions of the capacitance time $\tau_0 = C/g_L$.

Figure 10(a) compares the characteristic oscillatory time scale Δ_t of the channels response to a sinusoidal (3-Hz) current stimulus to $2\pi/\omega_1$ computed from the noise autocorrelation function at zero current, for five patches of membrane with different numbers of voltage-gated channels, as indicated. In each experiment the patch of membrane is first held at a zero current and its voltage fluctuations are monitored for at least 1 min. This measurement is used to compute the voltage autocorrelation function and hence derive ω_1. The same patch of membrane is then stimulated with a sinusoidal current of 2 pA rms at different frequencies (up to 3 Hz) for a few minutes. The voltage response of the system is recorded and then used to compute the average Δ_t between the first and second peaks that are identified in the voltage trace. The noticeable fact is that while Δ_t is almost constant, ω_1 varies between the different patches of membrane by more than a factor of 3. Figure 10(b) shows the same comparison between Δ_t and $2\pi/\omega_1$ derived from Monte Carlo simulations, as explained above, with a 3-Hz current stimulus for different numbers of channels, as indicated ($\tau_0 = 100$ msec). In the simulation, there is a linear relation between the two characteristic time scales. It shows that the difference in the number of channels cannot be the cause of the behavior depicted in Fig. 10(a). The inset to Fig. 10(b) shows Δ_t computed by solving numerically the dynamical two-state model [Eqs. (2) and (3)] with no noise (i.e., $\xi = 0$) and with a sinusoidal (3-Hz) driving current, as a function of the capacitance time scale. Comparing the depen-

dence on the capacitance time of Δ_t to that of $2\pi/\omega_1$ [see Fig. 6(b)] shows that the latter is more sensitive to it. The different patches of membrane in Fig. 10(a) may have different capacitance times since they are determined by the glass pipettes and the exposure of the glass tips to the solution (see the experimental methods above) and thus are not well controlled. The difference in the sensitivity of the characteristic time scales to τ_0 may explain the large variation of ω_1 in Fig. 10(a), but because each pair of measurements was done in the same patch of membrane, having the same parameters, the discrepancy between $2\pi/\omega_1$ and Δ_t in the experiments reflects the same deviation as (more than a factor of 2) observed in the simulations [Fig. 10(b)].

The exact value of Δ_t depends somewhat on the driving current amplitude for the range of amplitudes used in the numerical deterministic solution and the Monte Carlo simulations (we use a 5-pA amplitude in the numerical calculation), but the dependence on the capacitance time is the same. Accordingly, Δ_t from the numerical calculation deviates from the experimental results because of the differences in capacitance times and amplitudes of driving currents [16]. Note that both the numerical deterministic solution and the results of the Monte Carlo simulations, which include noise, agree fairly well. Thus the average time lapse Δ_t represents the deterministic response of the system. This deterministic measure is a noticeable effect, appearing to be stronger in the experiments than in the simulations, which marks an enhancement of the deterministic response of the system compared to the noise when driven by an external periodic stimulus. The fact that even for the simulation there is no agreement between the time scale appearing in the response to the external stimulus and the one characterized by the noise implies that a nonlinear effect takes over and determines the response time scale. We have checked by integrating the deterministic equations numerically that for a very-low-amplitude stimuli, Δ_t indeed converges to $2\pi/\omega_1$ of the noise trace. These low amplitudes do not allow us to extract the deterministic response out of the noise in the Monte Carlo simulations or experiments. We conclude, therefore, that the two-state system presented above exhibits nonlinear amplification of the deterministic response when driven by an external stimulus, although the range of voltage amplitudes of the deterministic response and that of the spontaneous noise are similar.

V. SMALL NUMBERS OF AVAILABLE CHANNELS: INACTIVATION DOMINANCE

So far we have seen a relatively simple picture of the system when there is a large number of available channels. In contrast, when the number of available voltage-gated channels is small, each branch of the kinetics may become important in determining the voltage dynamics. The result is that the dynamics of transmembrane voltage reflects the complex kinetics of the underlying channels. Let us look closely at the three-state model

$$C \underset{\beta(V)}{\overset{\alpha(V)}{\rightleftarrows}} O \underset{\delta}{\overset{\gamma}{\rightleftarrows}} I, \tag{21}$$

with single closed and inactive states. Just as in the two-state model, the $C \leftrightarrow O$ kinetics interacts with the transmembrane voltage and channels residing in these states are available for this interaction. The channels in the I states, however, are unavailable to respond to transmembrane voltage modulations. When I is significantly more populated than the available states each channel that relaxes to the available pool will cause large fluctuations in the transmembrane voltage. In the opposite situation, a large population in $C \leftrightarrow O$ ensures stability of the voltage and small fluctuations due to the feedback mechanism explained above. In fact, the sensitivity of the voltage to relaxation of channels from I to $C \leftrightarrow O$ is enhanced the larger the population in I relative to that in $C \leftrightarrow O$. The transition from $C \leftrightarrow O$ to I occurs only through the open (conducting) state of the channel, so the depletion of channels in the available states is more severe for small total numbers of channels since a larger fraction of them have to be open at any time to balance the leakage current.

Figure 11(a) shows the voltage histogram from a Monte Carlo simulation of 20 channels with the above kinetic scheme [Eq. (21)] of the three-state model. The probability of each channel to make a transition out of its state, at the time interval t, $t+dt$, is computed as before. This probability is compared to a random number, pulled out of a uniform distribution, and a transition is made if the random number is smaller. If the channel is in the open state, another random number is used to determine to which state the transition is made by using the ratio of the transition rates to the closed and inactive states [e.g., a transition to the closed state occurs if the random number is smaller than $\beta/(\beta+\gamma)$]. The histogram was computed with high resolution (0.6 mV/bin) to show the sensitivity of the voltage to channel fluctuations among states. Figure 11(b) shows the population of channels in the available states as a function of voltage for the same simulation. The simulation confirms the result that the potential change due to the inactivation of a single channel increases with the population of channels in the inactive states. Each peak in the histogram represents a step in sensitivity of the transmembrane voltage to the number of available channels, which can affect and respond to the voltage. This example demonstrates that the *effective* number of channels is actually a *dynamic variable*.

What determines the transmembrane voltage is then the distribution of channels between the $C \leftrightarrow O$ and I states rather than the total number of channels. Figure 12(a) shows a voltage trace recorded from a patch of membrane containing many voltage-gated potassium channels (~ 640). At the beginning of the trace, the holding current is zero and the transmembrane voltage is stabilized around -60 mV with low-amplitude fluctuations. At the point marked by the arrow, a positive [17] (8.3-pA, compared to 2-pA leakage current) dc current was applied to the membrane. This current forces an increase in the average number of open channels (from ~ 4 open channels at zero current to ~ 20 at 8.3 pA). As a result, the transmembrane voltage steadily drifts to more positive (depolarized) values, initially at an almost constant rate [Fig. 12(b)]. This steady change in the transmembrane potential reflects a steady loss of channels into the unavailable states of inactivation. Note that as the loss of channels progresses, the voltage drift is accelerated and the amplitude of fluctuations is increased. The accelerated loss

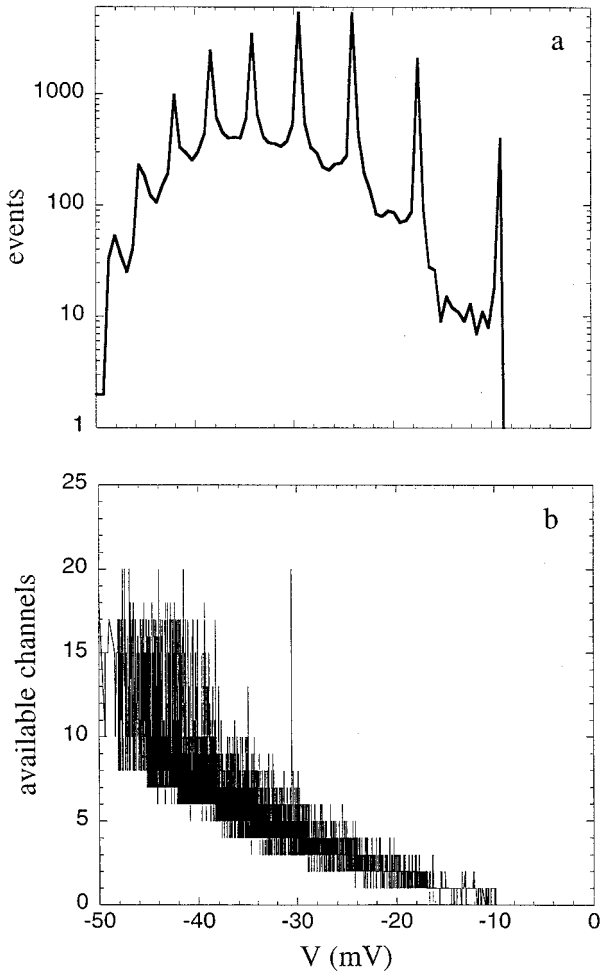

FIG. 11. (a) Histogram of voltage fluctuations calculated from a Monte Carlo simulation (see the text for details) of 20 channels, each with a three-state model $C \underset{\beta(V)}{\overset{\alpha(V)}{\rightleftarrows}} O \underset{\delta}{\overset{\gamma}{\rightleftarrows}} I$, where $\gamma = 5 \times 10^{-3}$ msec^{-1} and $\delta = 1 \times 10^{-3}$ msec^{-1} are the rates of transition into and out of the inactive state I, respectively, and the voltage-dependent rates $\alpha(V)$ and $\beta(V)$ are the same as in [14]. The rest of the parameters in this simulation are $g_k = 0.1$ in units of the leak conductivity (i.e., $g_L = 1$) and the membrane capacitance $\tau_0 = 100$ msec. (b) Number of available channels, i.e., channels in the voltage-dependent states ($C \leftrightarrow O$), as a function of the transmembrane voltage from the same simulation as in (a).

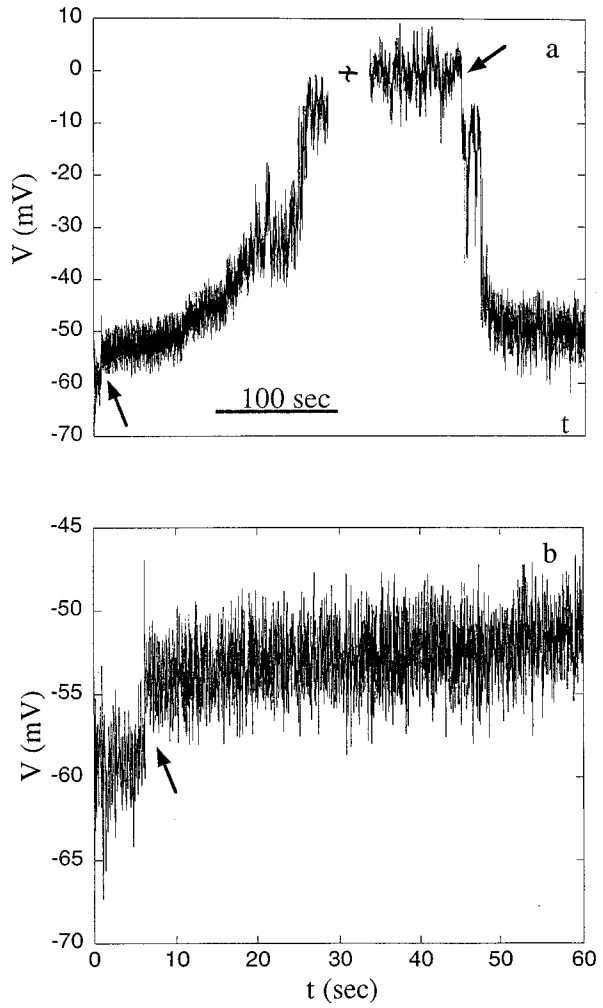

FIG. 12. (a) Voltage trace measured from a patch of membrane containing 640 channels. At the time marked by the left arrow the holding current was changed from 0 to 8.3 pA (the leakage current there is around 2 pA) and as a result, the voltage starts to drift to higher values due to the loss of channels into inactive states. After a few minutes, practically the whole pool of channels was inactive and the voltage exhibits large-amplitude fluctuations around the leak reversal potential (0 V), a behavior that mimics a membrane with a low density of channels. Note the acceleration in the voltage drift and in the increase of voltage fluctuations. At the right arrow the external current is set back to zero and the voltage relaxes back to low values due to a gradual relaxation of channels from the inactive states. (b) Initial drift in (a) enlarged to show that the voltage drift starts at a constant rate.

of channels can be understood from the previous argument: Increasing the voltage forces a larger fraction of channels to open, thereby increasing the loss rate. Actually, this means that even if we start with a large pool of available channels, a positive input current can effectively reduce them to very small numbers. This loss of channels into the inactive states is reversible, as shown by setting the external holding current back to zero at the second arrow and monitoring the relaxation of the transmembrane voltage.

The above example shows clearly that the ensemble of channels can move dynamically between the different regimes of high numbers of available channels to low numbers in a way that depends on the system's activity and the control parameters (total number of channels and input current). The initial rate of voltage change, as the holding current is changed from zero to a positive value, depends on the total number of channels in the membrane and the amplitude of the holding current. For larger numbers of channels, the initial rate of voltage change is smaller and it increases with the amplitude of the applied current. The hierarchy of time scales is such that the voltage-dependent transitions between the closed and open states are faster than the characteristic time of voltage adjustments (capacitance time of the membrane), which in turn is much faster than the relaxation time of channels from the inactive states. As a result, any change in the transmembrane voltage is instantaneously responded to by the available channels. Therefore, the channel distribution among the available states can be considered as in

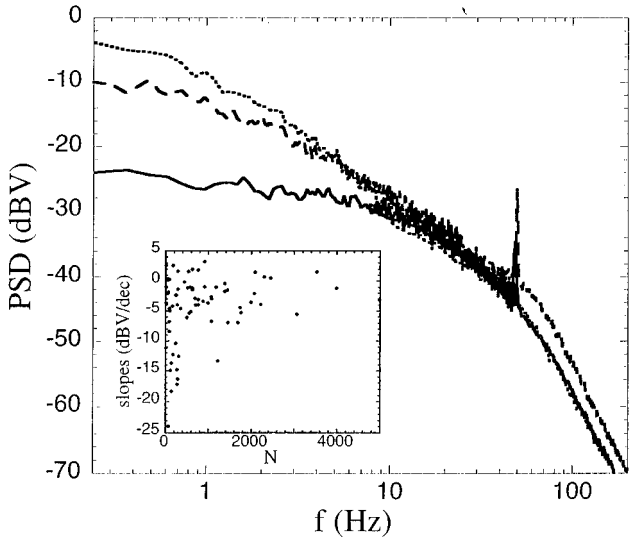

FIG. 13. (a) Power spectral densities (PSDs) for the voltage noise at zero holding currents, measured for patches of membrane containing 75 (dotted line), 130 (dashed line), and 5000 (solid line) channels. Note the change in the spectral characteristics at low frequencies as the number of channels is varied. Inset: summary of slopes of PSDs at low frequencies for different patches of membrane as a function of the number of channels. The spectrum converges to approximately a flat form (white noise) for large numbers of channels.

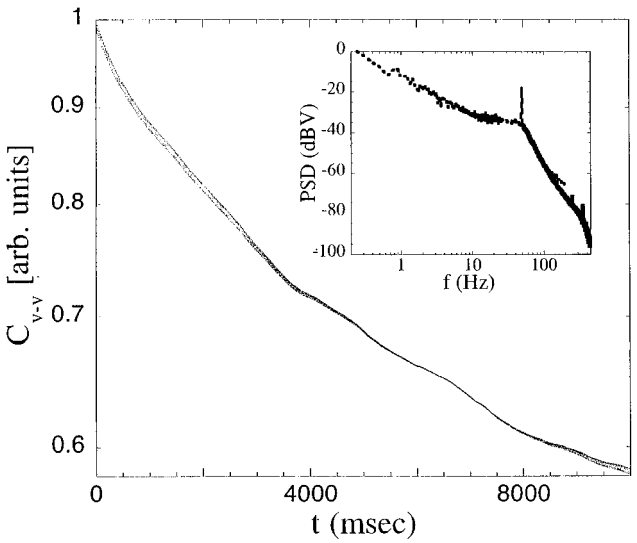

FIG. 14. Normalized voltage autocorrelation function, on a semi-logarithmic scale, averaged over 10 min (see the text for details), for a patch of membrane containing 75 channels at zero holding current. The inset shows the PSD for the same measurement.

steady state. If we force a certain average number of open channels (by the external holding current), some channels are lost into the inactive states at a constant rate and a larger *fraction* of available channels open. The voltage trace, then, follows the steady-state fraction of open channels $\alpha/(\alpha+\beta)$, which is linear for low enough voltages [see Fig. 1(b)]. The actual slope is determined by the total number of channels and the holding current, both of which determine the actual fraction of open channels at any given moment.

The spectral characteristics of voltage fluctuations for small numbers of channels reflect the competition between the fast, voltage-dependent rates of transition and the slow, voltage-independent ones. Figure 13 compares the power spectral density of voltage fluctuations, for three patches of membrane containing different numbers of voltage-gated channels at zero holding currents. In the high-frequency regime the spectrum falls as f^4, independently of the number of channels (see the power spectrum predicted by the two-state model [Eq. (18)] in the high-frequency limit), and reflects the fast, voltage-dependent kinetics. The ''knee'' that cuts this behavior is determined mainly by the capacitance of the system. The noticeable difference between the different spectra in Fig. 13 is at the low-frequency regime; an ensemble containing a large number of channels typically exhibits a flat spectrum at low frequencies, while one with a small number of channels exhibits a power-law spectrum, with larger slopes for smaller numbers of channels. The inset to Fig. 13 shows that the slopes of the power spectra at low frequencies vary over a wide range, up to f^2 for low numbers of channels, and exhibit approximately flat spectra for large numbers of channels.

The fact that the voltage dynamics for low numbers of available channels exhibits a wide range of time scales is also clearly observed in the voltage autocorrelation function for an ensemble with a small number of channels. The normalized voltage autocorrelation function for a patch of membrane containing 75 channels at zero current is shown in Fig. 14. The autocorrelation function is computed as before [Eq. (20)], averaged over 10 min. It exhibits relaxation processes over a wide range of time scales and cannot be fitted with a single exponential. Note the dramatic difference between this autocorrelation and the one presented in Fig. 4, for a large number of channels. We conclude that the kinetics of the inactive states and the relaxation of channels between the I and the $C \leftrightarrow O$ states exhibit a wide range of transition rates, which affect the voltage dynamics. The power law at the low-frequency regime of the spectrum (shown in the inset for the same patch of membrane) leads us to the same conclusion. Similarly, the current relaxations, measured for this channel in voltage-clamp experiments, cannot be fitted with a single exponential [4]. In principle, one needs to introduce more than one I state with a wide range of time scales to fit the measured autocorrelation function. The actual microscopic structure of the channel is not known, so such a detailed description is impossible. Figure 14 demonstrates, however, that when the available pool is depleted, many time scales show up in the voltage fluctuations and *a relatively detailed microscopic description of the underlying channel is needed in order to determine the macroscopic dynamics*. This stands in sharp contrast to the two-state model presented above for large numbers of channels, where only very crude information on the microscopic states is needed in order to describe the macroscopic dynamics.

VI. DISCUSSION

Controlled ensembles of voltage-gated ion channels provide us with an opportunity to study the collective dynamics of proteins. On the one hand, these proteins live in a Brownian noisy world and interact with the solution around them.

On the other hand, they are not free particles but are constrained within a membrane and are strongly influenced by it. The main field that couples the channels is the transmembrane voltage, but secondary effects could come from the membrane itself (e.g., mechanical modes). Our experiments detach the ion channels from any biochemical or intracellular effects, so the above-mentioned means of coupling are the only ones possible. We have not found any important coupling between the channels, other than the voltage. It is possible, however, that the type of experiments performed here are not sensitive enough to detect other modes of coupling.

In the ion-channel system it is impossible to go to the thermodynamic limit. Finite-size effects are always important. By varying the number of channels in the ensemble we are able to study the connection between the single-channel kinetics and the voltage dynamics, which reflects the collective response of the ensemble. There are two distinct phases. At high numbers of available channels, only two states of the channel play significant roles and single-channel fluctuations are amplified collectively to show up as relaxed oscillations of the voltage. In the opposite regime, of low numbers of available channels, all parts of the channel's kinetics interact with the voltage field, which in turn reflects the complex structure-function relationship of a single channel. The fact that the effective number of available voltage-gated ion channels is dynamically coupled to the electrical activity of the system demonstrates an important feature of biological systems: a direct coupling between the macroscopic phenomena and microscopic kinetics of the underlying proteins, on many scales. An intriguing fact is that the ensemble of channels can move dynamically between the different regimes, depending on its history of activity. A natural cell containing many different ion channels has a much richer range of possibilities. The biological system can, by choice, use its available phase space (the microscopic degrees of freedom of the underlying proteins) or apply constraints on it so that only a few degrees of freedom interact with the macroscopic field. This ability of the biological system enables it to fulfill its function. The fact that the details of the single protein kinetics are important in the description of large-scale phenomena of cells (and networks of cells) poses a nontrivial challenge in our quest to grasp biological phenomena.

ACKNOWLEDGMENTS

This research was supported by Grant No. 94-00262 from the United States–Israel Binational Science Foundation, Jerusalem, Israel. We thank V. Lyakhov for technical assistance and A. Libchaber, S. Marom, N. Cohen, Y. Soen, and D. Kandel for helpful discussions.

[1] B. Hille, *Ionic Channels of Excitable Membranes*, 2nd ed. (Sinauer, Sunderland, 1992).

[2] *Single-Channel Recording*, 2nd ed., edited by B. Sakmann and E. Neher (Plenum, New York, 1995).

[3] T. Hoshi, W. N. Zagotta, and W. R. Aldrich, Science **250**, 533 (1990); S. Marom, S. A. N. Goldstein, J. Kupper, and I. Levitan, Receptors Channels **1**, 81 (1993).

[4] S. Marom, H. Salman, V. Lyakhov, and E. Braun, J. Membrane Biol. **154,** 267 (1996).

[5] H. Salman, Y. Soen, and E. Braun, Phys. Rev. Lett. **77**, 4458 (1996).

[6] T. Hoshi, W. N. Zagotta, and W. R. Aldrich, Neuron **7**, 547 (1991).

[7] S. A. N. Goldstein and C. Miller, Biophys. J. **62**, 5 (1992).

[8] See S. Marom and I. B. Levitan, Biophys. J. **67**, 579 (1994), and references therein.

[9] G. Yellen, M. E. Jurman, T. Abramson, and R. MacKinnon, Science **251**, 939 (1991).

[10] H. Lecar and R. Nossal, Biophys. J. **11**, 1068 (1971).

[11] A. E. Siegman, *Lasers* (University Science, Mill Valley, CA, 1986), p. 958.

[12] For the cases of *stochastic resonance* see, for example, K. Wiesenfeld and F. Moss, Nature (London) **373**, 33 (1995); E. Pantazelou, F. Moss, and D. Chiavlo, in *Noise in Physical Systems and* $1/f$ *Fluctuations*, edited by P. Handel and A. Chung, AIP Conf. Proc. No. 285 (AIP, New York, 1993), p. 549; S. M. Bezrukov and I. Vodynoy, Nature (London) **378**, 362 (1995); P. Jung and G. Mayer-Kress, Phys. Rev. Lett. **74**, 2130 (1995). For the case of *resonant activation* see, for example, C. R. Doering and J. C. Gadoua, *ibid.* **69**, 2318 (1992); P. Reimann, *ibid.* **74**, 4576 (1995).

[13] R. Kubo, M. Toda, and N. Hashitsume, *Statistical Physics II, Nonequilibrium Statistical Mechanics* (Springer-Verlag, Berlin, 1985).

[14] For all the simulations in this manuscript we use the voltage-dependent rates as measured in [4]: $\alpha=0.03(V+146)/\{1-\exp[-0.8(V+46)]\}$ and $\beta=-0.02V\exp[-0.023(V+148)]$ in msec^{-1} (V is in mV).

[15] W. H. Press, B. P. Flannery, S. A. Teukolsky, and W. T. Vetterling, *Numerical Recipes in Fortran*, 2nd ed. (Cambridge University Press, Cambridge, 1992).

[16] Interestingly, to extract the response Δ_t in the Monte Carlo simulations one needs to use higher current amplitudes than those used experimentally. It may mark a stronger nonlinear effect in the experiment than predicted by the model.

[17] A positive holding current increases the number of open channels that conduct the necessary potassium current to balance it.